

TagSplat: Topology-Aware Gaussian Splatting for Dynamic Mesh Modeling and Tracking

Hanzhi Guo

Beijing Institute of Technology
Beijing
hanzhiguo@bit.edu.cn

Dongdong Weng

Beijing Institute of Technology
Beijing
crgj@bit.edu.cn

Mo Su

Soul Shell Technology Co., Ltd
Beijing
schumer425@126.com

Yixiao Chen

Beijing Institute of Technology
Beijing
yxchenggeorge@163.com

Dongye Xiaonuo

Beijing Institute of Technology
Beijing
dyxn@bit.edu.cn

Chenyu Xu

Soul Shell Technology Co., Ltd
Beijing

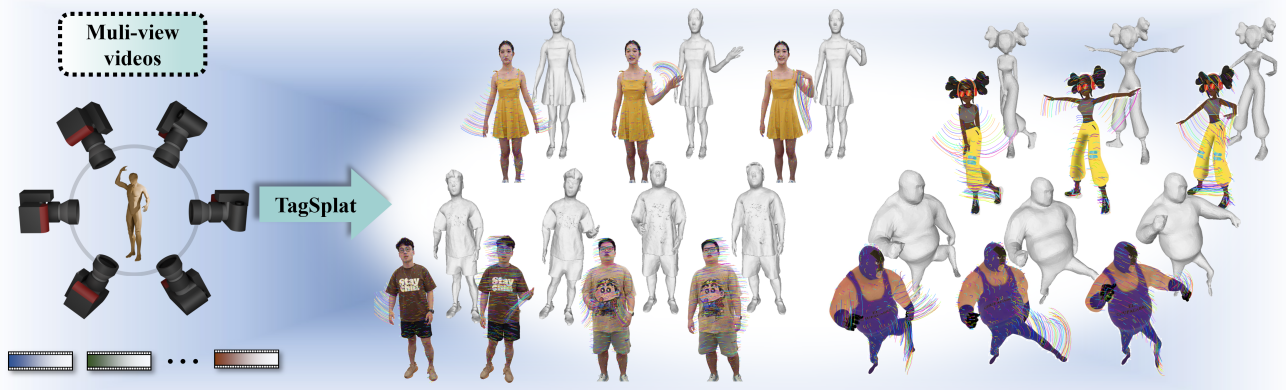


Figure 1. Our method reconstructs dynamic humans from multi-view videos. Our topology-aware strategy produces topology-consistent Gaussian and mesh sequences, enabling accurate dynamic reconstruction and tracking.

Abstract

Topology-consistent dynamic model sequences are essential for applications such as animation and model editing. However, existing 4D reconstruction methods face challenges in generating high-quality topology-consistent meshes. To address this, we propose a topology-aware dynamic reconstruction framework based on Gaussian Splatting. We introduce a Gaussian topological structure that explicitly encodes spatial connectivity. This structure enables topology-aware densification and pruning, preserving the manifold consistency of the Gaussian representation. Temporal regularization terms further ensure topological coherence over time, while differentiable mesh rasterization improves mesh quality. Experimental results demonstrate that our method reconstructs topology-consistent mesh sequences with significantly higher accuracy than existing approaches. Moreover, the resulting meshes enable precise 3D

keypoint tracking. Project page: <https://haza628.github.io/tagSplat/>

1. Introduction

The animation industry relies on a comprehensive mesh-centered toolchain for rendering, skinning, and editing. Efficiently reconstructing dynamic mesh sequences with consistent topology remains a key challenge bridging computer vision and graphics [2, 9, 12, 13, 42, 46]. Such topology-consistent meshes are crucial for downstream tasks. In traditional production pipelines, they are created manually or via optical-flow-based retopology of high-resolution per-frame reconstructions. Unlike costly manual pipelines, Gaussian Splatting provides an efficient explicit representation for high-quality 3D reconstruction[20]. By explicitly modeling geometry and appearance with 3D Gaussians, it achieves fast reconstruction, high-fidelity render-

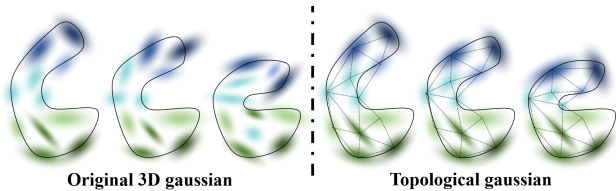


Figure 2. Illustration of the Gaussian topology structure. Each Gaussian primitive is connected via manifold edges. Compared with the original 3D Gaussians, our structure constrains the relative positions and rotations of neighboring Gaussians. This method enables training Gaussian and mesh models with consistent topology.

ing, and easy editability. Unlike implicit representations [30, 31, 34], it preserves a point cloud structure, allowing seamless integration with standard geometric processing.

Recent studies have started exploring dynamic mesh generation from Gaussian Splatting. A 3D Gaussian representation can be treated as a point cloud. Meshes can then be reconstructed from this point cloud using methods such as Poisson reconstruction or depth-based techniques. Several works have attempted to reconstruct dynamic mesh sequences from Gaussian Splatting[25, 49, 50]. Reconstructed meshes are generated independently for each frame due to the lack of temporal consistency constraints. This independence leads to frame-wise variations in topology. As a result, downstream tasks such as skeleton binding and keypoint tracking remain fundamentally challenging. Therefore, how to generate topology-consistent dynamic mesh sequences remains an open problem.

To address the challenge of reconstructing topology-consistent mesh sequences in Gaussian Splatting, we propose a Gaussian topological structure, as illustrated in Fig. 2. Based on this structure, we propose a topology-aware 3D Gaussian densification and pruning process. The topology is automatically updated whenever Gaussian primitives are added or removed. This adaptive topology update ensures that the manifold structure is preserved during 3D Gaussian densification. The mesh vertices of each frame follow the positions of the corresponding 3D Gaussians, and combined with the Gaussian topology, the mesh model of the target object can be obtained. To ensure temporal coherence across dynamic sequences, we incorporate regularization terms that preserve the relative positions and rotations of each Gaussian primitive within its 1-ring neighborhood. We also employ a differentiable mesh rasterizer to improve geometric accuracy. This combination allows not only topology-consistent mesh reconstruction but also 3D keypoint tracking by preserving the relative positions of keypoints on the mesh surface over time. Our method is the first to maintain manifold topology through dynamic Gaussian updates, enabling the reconstruction of topology-consistent meshes and accurate tracking.

Our main contributions are summarized as follows:

- We propose a Gaussian topology representation that bridges the gap between Gaussian Splatting and mesh models, enabling fast and consistent conversion.
- We propose an adaptive topology-based densification and pruning method that preserves the manifold topology during the Gaussian densification and pruning processes.
- We design temporal consistency constraints based on a Gaussian topology structure to ensure temporally smooth and topology-consistent Gaussian distributions in dynamic sequences.
- We build an end-to-end framework for dynamic reconstruction and 3D tracking, providing a practical and low-cost solution for animation and model editing tasks.

2. Related works

2.1. Neural 3D reconstruction and rendering

Neural implicit representations refer to techniques that use neural networks to implicitly model 3D shapes and scene attributes. The most notable example is NeRF[31], which optimizes voxel density and radiance from multi-view images to achieve high-fidelity novel view synthesis. Following NeRF, many works have focused on improving representation efficiency and detail quality. Instant-NGP[33] introduced hash-grid encoding to enable high-resolution NeRF training within minutes; Plenoxels[11] directly optimize voxel attributes in a sparse voxel grid, avoiding the overparameterization of neural networks.

To better adapt to complex geometry, NeuS[42] incorporated signed distance function (SDF) constraints and optimized surface normal consistency through differentiable rendering. VolSDF[47] combined volumetric rendering with SDF to guide volume density concentration on differentiable surfaces. These methods achieve excellent results in static scene modeling but offer limited support for dynamic scenes or editable meshes.

Compared to NeRF, Gaussian Splatting provides an explicit and lightweight-optimizable 3D representation. Gaussian splatting[20] systematically proposed 3D Gaussian splatting rendering, converting NeRF volumetric integration into differentiable rendering of continuous Gaussian distributions. This approach enables high-quality novel view synthesis within minutes and real-time performance on mobile devices.

The main advantage of Gaussian Splatting lies in explicitly modeling each Gaussian primitive’s position, covariance, and color attributes, which are easy to edit, merge, and densify. Numerous extensions of Gaussian Splatting have been explored[6, 10, 16, 39, 48]. Dynamic scene reconstruction based on Gaussian Splatting has seen a surge of research efforts. Some studies focus on 4D reconstruction, recovering dynamic Gaussian representations of scenes from single-view or multi-view videos[17–19, 29]. Others con-

centrate on human performance modeling, aiming to produce highly realistic and controllable human avatars[15, 24, 32, 38, 45]. There are also approaches that introduce physical constraints into the Gaussian Splatting framework to learn physically consistent dynamic objects[1, 8, 44]. In addition, some works address model compression to improve the efficiency and practicality of Gaussian Splatting in dynamic settings[4, 5, 7, 26, 27].

Although Gaussian Splatting enables high-quality rendering, current animation production pipelines remain fundamentally mesh-based. Since Gaussian Splatting synthesizes images through 3D Gaussian functions, it still lacks mature solutions for lighting, deformation, and editing. Consequently, its integration into computer animation remains limited. Nonetheless, Gaussian Splatting provides a new perspective and valuable inspiration for advancing mesh reconstruction research.

2.2. Mesh Reconstruction

Mesh models have long been a central representation in 3D computer graphics. For dynamic scenes, reconstructing topology-consistent meshes is crucial for tasks such as motion control and model editing. Traditional NeRF-based methods[35–37, 40] struggle to impose explicit topological constraints on dynamic objects, leading to reconstructions that lack temporal consistency. Although mesh models can be extracted for each frame using methods such as Marching Cubes [28] or Marching Tetrahedra[41], these approaches remain essentially frame-wise static reconstructions and do not ensure continuity across time. Recent works therefore aim to achieve high-fidelity modeling while preserving consistent spatial structure.

To address these issues, several Gaussian-based mesh reconstruction approaches have been proposed. Topo4D[23] binds Gaussians to the vertices of a static template mesh and drives their positional deformation across frames while maintaining their topological relationships. However, this method is limited to head models and relies on a high-quality Metahuman template. GauSTAR[50] reconstructs and tracks dynamic geometry using Gaussian Splatting guided by optical flow, yet its preprocessing pipeline is complex and difficult to deploy in production environments. More recent methods have made progress in both simplicity and reconstruction quality. DG-Mesh[25] attaches Gaussians to a mesh representation and can automatically reconstruct dynamic meshes, while Dynamic 2DGS[49] incorporates 2D Gaussian primitives to achieve more accurate mesh reconstruction.

It is worth noting that although the aforementioned methods have made progress in temporal consistency and mesh reconstruction, they are still unable to produce topology-consistent mesh sequences. Most existing approaches reconstruct meshes by applying Poisson reconstruction or

similar techniques to the point cloud of each frame. This makes it difficult to enforce consistent topology across frames, or even to maintain a fixed number of vertices. As a result, the reconstructed meshes are often unsuitable for downstream tasks such as animation production.

3. Method

To reconstruct a sequence of topology-consistent mesh models and enable robust keypoint tracking, we propose a topology-constrained dynamic Gaussian Splatting framework built upon standard 3D Gaussians (Sec. 3.1). Our pipeline starts by initializing Gaussians from the mesh reconstructed in the first frame. By introducing a manifold topology prior, we convert the initial mesh into a structured Gaussian point cloud. Based on this, we design a topology-aware Gaussian densification strategy that supports both training and refinement of Gaussians while preserving the underlying manifold structure(Sec. 3.2). For subsequent frames, we enforce temporal coherence of Gaussian parameters via 1-ring neighborhood regularization, ensuring consistent topology across the entire sequence (Sec. 3.3). Once the dynamic Gaussians are fully optimized, we obtain a sequence of topology-consistent meshes and support stable 3D keypoint tracking (Sec. 3.4). The overall pipeline is illustrated in the Fig. 3.

3.1. 3D Gaussian splatting

3D Gaussian splatting represent an explicit 3D representation method that is trained using multi-view images of the target object along with corresponding camera parameters. The target object is modeled by a large number of 3D Gaussians, each parameterized by its position μ , covariance matrix Σ , and color c . The Gaussian function is defined as follows:

$$G(x) = e^{-\frac{1}{2}(x-\mu)^T \Sigma^{-1}(x-\mu)} \quad (1)$$

The covariance matrix Σ must be positive semi-definite. Therefore, it is decomposed into two components: a rotation matrix R representing orientation, and a scaling matrix S representing scale. To ensure that the covariance matrix remains positive semi-definite during gradient descent optimization, it is defined as follows:

$$\Sigma = R S S^T R^T \quad (2)$$

For 2D image rendering, the color value c_i of each Gaussian at a pixel location is computed using spherical harmonics. The weight α_i is calculated based on opacity and the 2D Gaussian distribution. The pixel color C is obtained by compositing k 2D Gaussians in depth order as follows:

$$C = \sum_{i=1}^k \alpha_i \prod_{j=1}^{i-1} (1 - \alpha_j) c_i \quad (3)$$

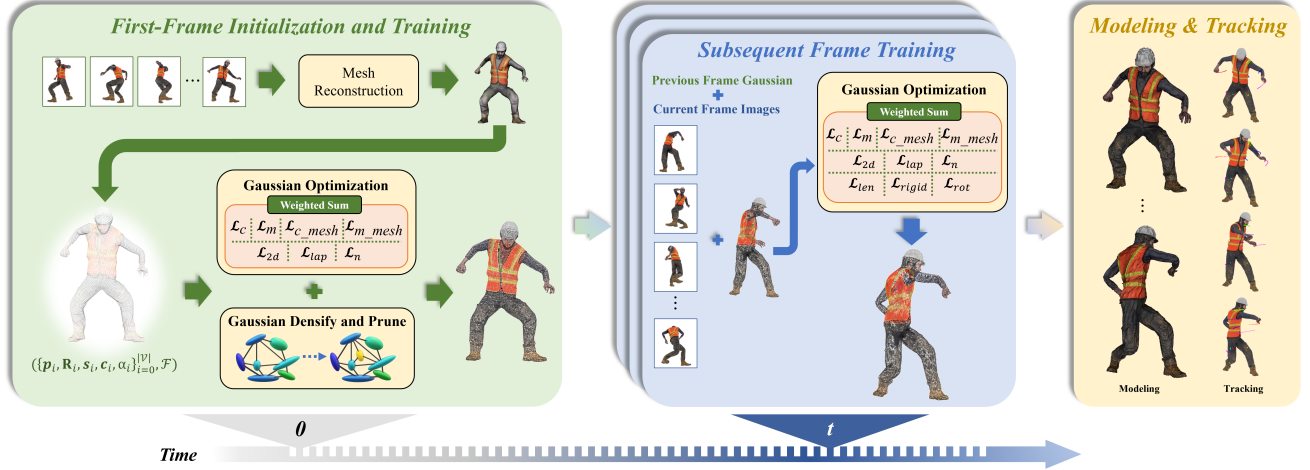


Figure 3. Overview of our pipeline. We first reconstruct an initial mesh from multi-view images and convert it into a Gaussian point cloud with manifold topology. A topology-aware densification and pruning strategy is then applied to refine the Gaussian representation while preserving surface connectivity. Temporal consistency constraints are introduced to enforce coherent deformation of Gaussians across frames. Finally, topology-consistent Gaussian and mesh sequences are obtained, enabling accurate 3D keypoint tracking.

3.2. Topology-Aware Gaussian Initialization and Optimization

First, the topological structure of the Gaussian model needs to be optimized. To ensure correct topology reconstruction, this stage uses a canonical pose (e.g., A-pose or equivalent pose) as the initial reference. For the datasets we use, the first frame provides a suitable initial pose, enabling a stable topology optimization process. We initialize Gaussian primitives from a high-quality multi-view reconstructed mesh of the first frame. Each Gaussian is associated with a vertex, inheriting its position, color, and connectivity to preserve topology. Rotation, scale, and opacity parameters are also initialized to roughly align the Gaussians with the mesh surface. This initialization provides a topology-consistent starting point for subsequent optimization, ensuring better convergence and reconstruction fidelity.

Gaussian Optimization

To achieve accurate reconstruction in a canonical pose, we optimize several losses. Color losses \mathcal{L}_c and $\mathcal{L}_{\text{mesh},c}$ align rendered images with ground truth. Mask losses \mathcal{L}_m and $\mathcal{L}_{\text{mesh},m}$ enforce coverage of the target region. 2D scale loss \mathcal{L}_{2d} improves Gaussian fitting to the object surface. Laplace smoothness \mathcal{L}_{lap} reduces local spikes, and normal consistency \mathcal{L}_n aligns Gaussian orientations with mesh normals. Joint optimization yields a detailed Gaussian representation with consistent topology.

Given the ground-truth image I_{gt} and the Gaussian Splatting rendering I_{gs} , we use the 3DGS[20] image loss.

$$\mathcal{L}_c^{gs} = 0.8 \cdot \|I_{gs} - I_{gt}\| + 0.2 \cdot \mathcal{L}_{\text{ssim}}(I_{gs}, I_{gt}) \quad (4)$$

We use a mask loss. I_m represents the rendering with Gaussian colors set to white and opacities set to 1, and I_{mask} represents the ground-truth mask, which can be extracted using the SAM[21]. The loss is defined as:

$$\mathcal{L}_m^{gs} = 0.8 \cdot \|I_m - I_{\text{mask}}\| + 0.2 \cdot \mathcal{L}_{\text{ssim}}(I_m, I_{\text{mask}}) \quad (5)$$

A mesh is constructed from the current Gaussian vertices and their topology, with Gaussian RGB values assigned as vertex colors. The mesh is rendered differentially using Nvdiffrast[22]. The mesh losses $\mathcal{L}_c^{\text{mesh}}$ and $\mathcal{L}_m^{\text{mesh}}$ are computed analogously to the Gaussian image losses.

To enable Gaussian primitives to better represent the surface of the target object, we impose a constraint on the scale along the z -axis during training, encouraging it to be as small as possible. The smaller the scale along the z -axis, the closer the trained Gaussian model fits the target object shape[23]. The scale constraint loss function we use is defined as:

$$\mathcal{L}_{2d} = \sum_{i=1}^k s_z^i \quad (6)$$

where k is the total number of Gaussians. s_z^i represent the scale along the z -axis.

In addition to constraining the Gaussian z -axis scaling parameter, we adopt a Laplacian smoothness term as a regularization to penalize local spatial discontinuities[25]. This encourages smoother Gaussian positions and suppresses spiky artifacts by penalizing local spatial variations.

$$\mathcal{L}_{\text{lap}} = \frac{1}{k} \sum_{i=1}^k \|\delta_i\|^2, \quad \delta_i = \mu_i - \frac{1}{|m|} \sum_{j=1}^m \mu_j \quad (7)$$

where, m denotes the number of 1-ring neighbors of Gaussian primitive i , and μ_i denotes its position.

We further introduce a normal consistency loss. For any Gaussian primitive, the vertex normal at the corresponding vertex, computed from the mesh model, is denoted as \mathbf{n}^{mesh} . We define the z -axis direction of the Gaussian's rotation parameter as the Gaussian normal direction, denoted as \mathbf{n}^{gs} . The normal consistency loss is formulated as:

$$\mathcal{L}_n = \sum_{i=1}^k \|\mathbf{n}_i^{gs} - \mathbf{n}_i^{mesh}\| \quad (8)$$

Finally, all the aforementioned loss terms are combined through a weighted summation to construct the overall loss function for the first-frame Gaussian model, which guides the training of both Gaussian parameters and the topology structure.

Topology-preserving densification and pruning

Our method builds upon the original Gaussian densification and pruning strategies by introducing an update approach that maintains manifold topology. The original Gaussian method determines point addition or removal solely based on local properties of Gaussian points (e.g., projection gradients, opacity, scale). The newly added or removed points are treated independently without explicit connectivity between points. As a result, the manifold structure of the geometric surface is prone to disruption during iterations.

To this end, while retaining the original Gaussian criteria for selecting points to densify or prune, we design a topology maintenance mechanism specifically for the addition and removal operations. The densification process is illustrated in Fig. 4. During densification, for any triangle whose projection gradient exceeds a threshold, we insert a new Gaussian point in the parameter space. Its attributes are computed as the average of the three vertex Gaussian parameters. Simultaneously, the original triangle is subdivided into three new triangles: $(\mu_0, \mu_1, \mu_{new})$, $(\mu_1, \mu_2, \mu_{new})$, $(\mu_2, \mu_0, \mu_{new})$. The face set is updated accordingly, thereby maintaining the Gaussian topological connectivity during densification.

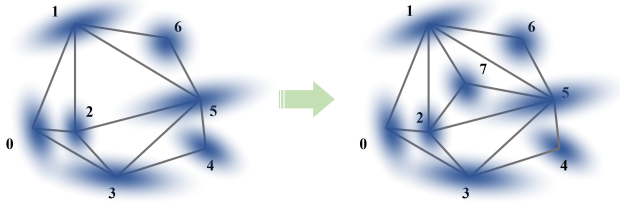


Figure 4. Topology-preserving densification.

During the pruning stage, we first identify Gaussian points to be removed based on the original criteria. Unlike the original gaussian splatting, we adopt a topology-

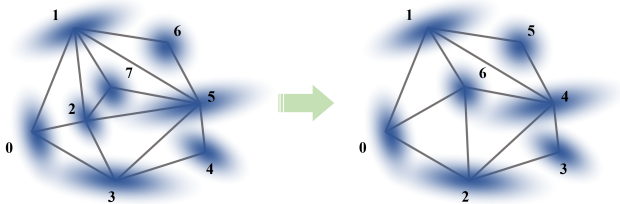


Figure 5. Topology-preserving pruning.

preserving merging strategy with the nearest neighbor to maintain the manifold, as illustrated in Fig. 5. Inspired by the edge collapse strategy proposed by Hoppe et al.[14], we design an edge collapse cost function tailored for the Gaussian topology structure. The function integrates geometric and attribute errors in a weighted manner to minimize both geometric and visual loss during the simplification process. Specifically, for each Gaussian primitive to be pruned, we compute the collapse cost for all edges connecting it to its 1-ring neighboring primitives. The geometric error E_g is measured by the Euclidean distance between their centers, while the attribute error E_a is computed based on color differences. The overall collapse cost C is then obtained by combining the two:

$$C = \omega_g \cdot \|\mathbf{p}_i - \mathbf{p}_j\| + \omega_a \cdot \|\mathbf{c}_i - \mathbf{c}_j\| \quad (9)$$

where ω_g and ω_a are the respective weighting coefficients used to unify the scales of different error terms. The edge with the minimal cost C is selected for collapse, thereby achieving efficient simplification while preserving topological consistency.

By incorporating this topology-aware update strategy into both densification and pruning, the Gaussian distribution is adaptively refined while the manifold structure of the surface is preserved throughout canonical-space optimization. This enables coherent and controllable geometric modeling. To maintain consistent topology during dynamic reconstruction, densification and pruning are applied only in the canonical space.

3.3. Topology-Consistent Gaussian Training

In the 3DGS training process, individual Gaussians have no explicit relationships. This leads to disordered outputs and uncontrolled relative positions, which compromise temporal consistency and continuity. To address this, we establish temporal consistency loss functions for subsequent frames. The edge length consistency loss \mathcal{L}_{len} preserves the spatial structure. The rigidity constraint loss \mathcal{L}_{rigid} leverages the 1-ring neighborhood to suppress local deformations. The rotation consistency loss \mathcal{L}_{rot} ensures smooth rotational changes across frames. By jointly optimizing these losses, temporal coherence is maintained throughout multi-frame training.

To constrain the relative positions of Gaussians, we propose a Gaussian topology edge length consistency loss, which enforces continuity of distances between adjacent Gaussians across frames:

$$\mathcal{L}_{len} = \sum_{i=1}^{k_l} \|l_{t,i} - l_{t-1,i}\| \quad (10)$$

where k_l is the number of edges. For a Gaussian i , let $l_{t,i}$ denote the edge length at frame t based on the topology.

To better regulate the motion of Gaussian distributions and preserve topological information, we extend the Gaus-

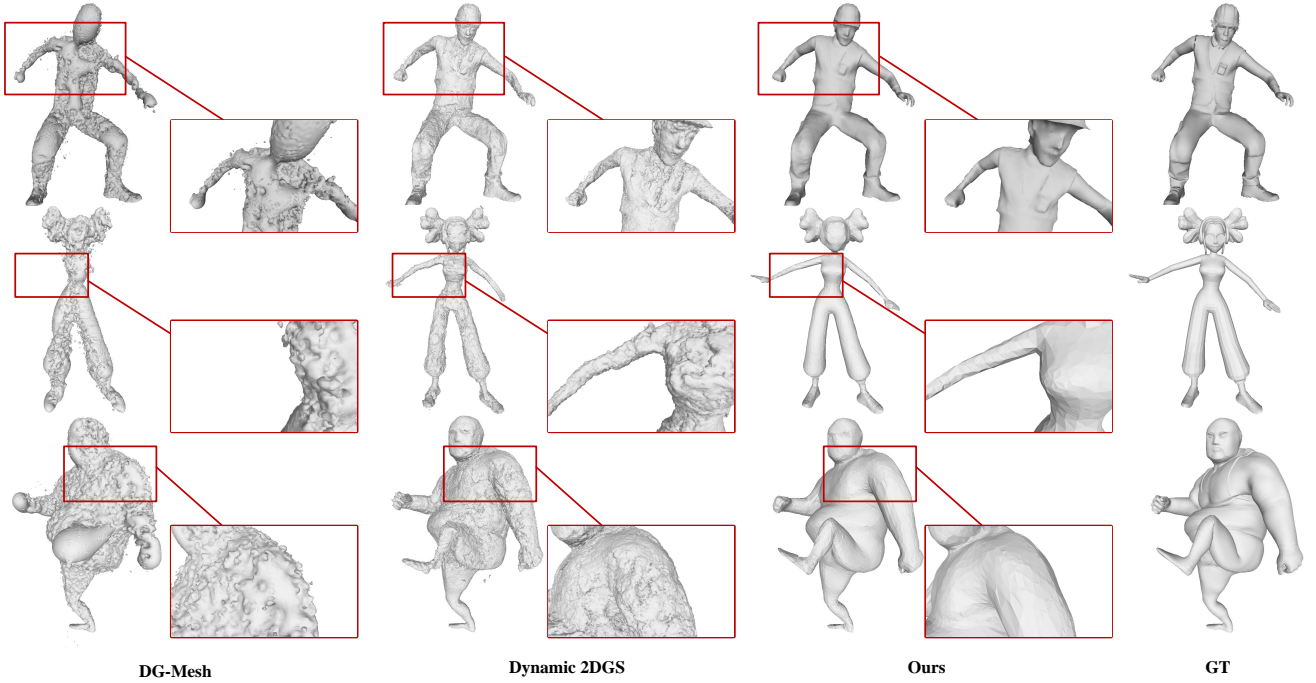


Figure 6. Mesh reconstruction comparison on the MIX-TAG dataset.

sian edge length loss. Following [29], we refine both the rigid loss and the rotation loss using the 1-ring neighborhood. The rigid loss is defined as follows:

$$\mathcal{L}_{i,j} = \|(\boldsymbol{\mu}_{j,t-1} - \boldsymbol{\mu}_{i,t-1}) - \Delta\mathbf{R}_t(\boldsymbol{\mu}_{j,t} - \boldsymbol{\mu}_{i,t})\| \quad (11)$$

$$\mathcal{L}_{rigid} = \sum_{i=1}^k \sum_{j=1}^m \omega_{i,j} \mathcal{L}_{i,j} \quad (12)$$

where $\Delta\mathbf{R}_t = \mathbf{R}_{i,t-1} \mathbf{R}_{i,t}^{-1}$, $\omega_{i,j} = \exp(-\lambda_w \cdot l_{i,j})$, and m is the number of 1-ring neighbors of μ_i . $\mathbf{R}_{i,t}$ denotes the rotation matrix of Gaussian primitive i at frame t .

The rotation loss based on the 1-ring neighborhood is given by:

$$\mathcal{L}_{rot} = \sum_{i=1}^k \sum_{j=1}^m \omega_{i,j} \| \mathbf{q}_{j,t} \otimes \mathbf{q}_{j,t-1}^{-1} - \mathbf{q}_{i,t} \otimes \mathbf{q}_{i,t-1}^{-1} \| \quad (13)$$

where \mathbf{q} denotes the normalized quaternion. \mathbf{q}^{-1} denotes the conjugate of the quaternion. \otimes denotes quaternion multiplication.

The loss function for training Gaussians in subsequent frames is a weighted sum of the three topology constraints above and the first frame training loss.

3.4. Modeling and Tracking

After training, we obtain a sequence of Gaussians with consistent topology. The position parameters of each Gaussian serve as the vertex positions of the mesh, while the learned manifold topology defines the connectivity. Using the Gaussian positions as vertices, a mesh can be generated for each frame. By first reducing the 3D spherical harmonic parameters to a single dimension and then converting it to RGB values, colored mesh models can be exported from Gaussian Splatting.

Any 3D point on the reconstructed mesh surface can be represented by a set of barycentric coordinates and a triangle face index. Since we obtain a sequence of meshes with consistent topology, the parameterization of these points applies to the mesh models of all frames. Thus, the trajectory of any target point can be tracked across all frames using this representation.

4. Experiments

4.1. Data Preparation

We evaluated our algorithm on both synthetic and real datasets. First, we rendered a dataset named MIX-TAG using motion data downloaded from Mixamo to evaluate modeling and tracking performance. The images in the dataset have a resolution of 1080×1080, with each subject captured from 42 different viewpoints. MIX-TAG provides ground-truth mesh, enabling quantitative evaluation of key-point tracking accuracy and mesh reconstruction accuracy. For real data, we trained and tested on the TalkBody4D dataset, introduced in Taoavatar [3]. It contains 4D human motion data captured by 59 precisely calibrated RGB cameras at 20 FPS, with a resolution of 3000×4000 pixels. In our experiments, we used only 30 of these camera views for training and evaluation. Our algorithm is implemented in PyTorch and trained on an NVIDIA RTX 3090 GPU with 24GB of memory. For the initial mesh reconstruction, we adopt the NeuS2[43] method.

4.2. Comparison

We conducted comparative experiments on reconstruction accuracy and tracking precision using the MIX-TAG

		PSNR _{g_s} ↑	SSIM _{g_s} ↑	LPIPS _{g_s} ↓	CD ↓	EMD ↓	Tracking MSE ↓	T-C Mesh
Boxer	Dynamic 3DGS	30.56	0.97	0.026	✗	✗	0.000676	✗
	DG-Mesh	22.46	0.95	0.080	1.48	0.29	0.013502	✗
	Deformable-GS	34.38	0.98	0.016	✗	✗	0.006631	✗
	Dynamic 2DGS	34.27	0.97	0.018	0.47	0.13	0.009148	✗
	Ours	34.76	0.98	0.15	0.32	0.010	0.000569	✓
Dancer	Dynamic 3DGS	30.19	0.97	0.021	✗	✗	0.000329	✗
	DG-Mesh	19.27	0.94	0.093	10.31	0.43	0.019222	✗
	Deformable-GS	19.08	0.94	0.081	✗	✗	0.042462	✗
	Dynamic 2DGS	27.45	0.98	0.030	0.75	0.13	0.042436	✗
	Ours	34.61	0.98	0.010	0.24	0.088	0.000101	✓
Worker	Dynamic 3DGS	29.22	0.95	0.031	✗	✗	0.000226	✗
	DG-Mesh	19.13	0.90	0.11	7.15	0.35	0.048107	✗
	Deformable-GS	31.93	0.96	0.026	✗	✗	0.028535	✗
	Dynamic 2DGS	31.86	0.96	0.023	0.45	0.12	0.057903	✗
	Ours	32.17	0.97	0.021	0.39	0.10	0.000218	✓

Table 1. Rendering, modeling, and tracking quality comparison on the MIX-TAG dataset. T-C Mesh indicates whether a method can reconstruct a topology-consistent mesh sequence.

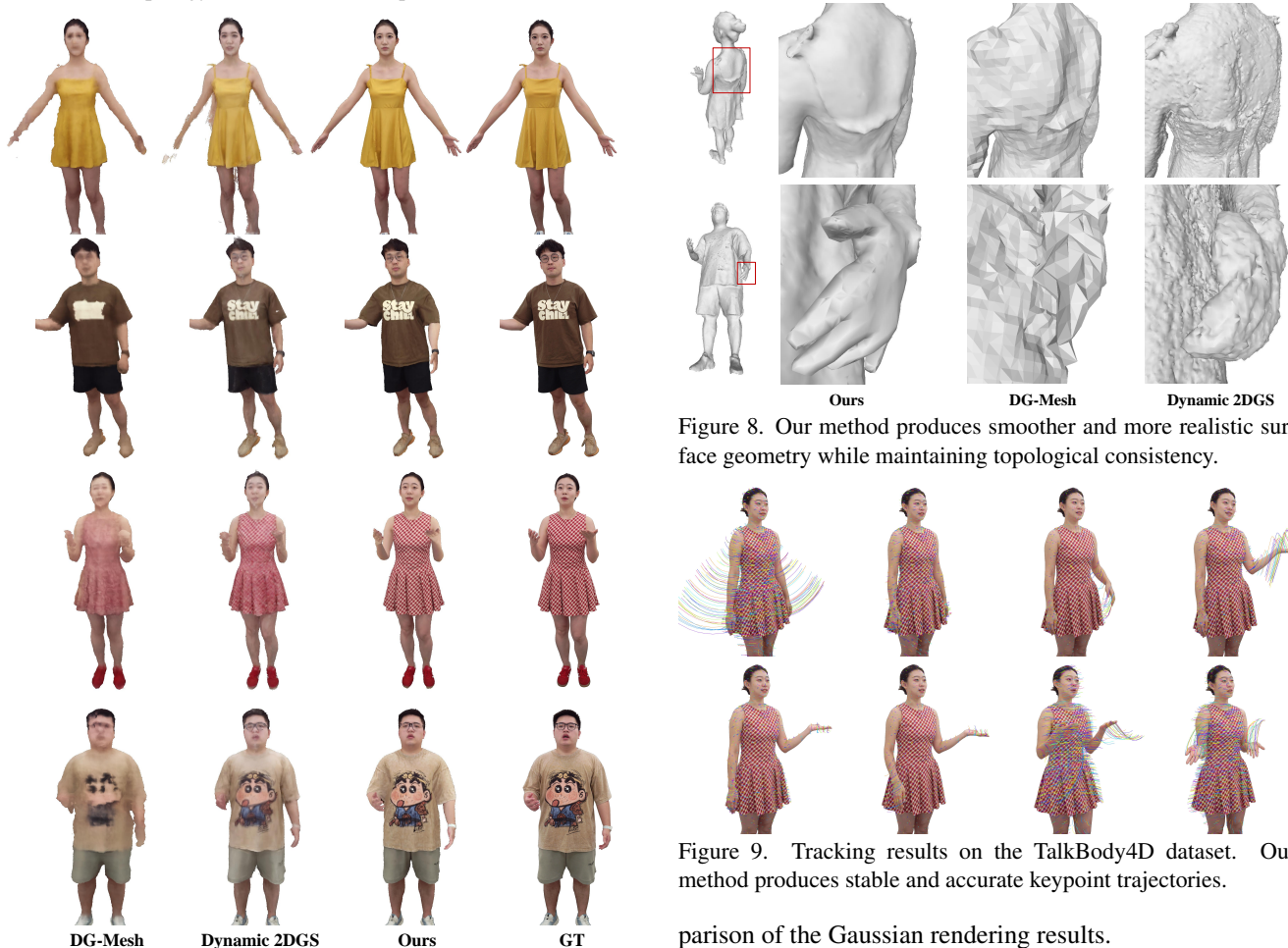


Figure 7. Mesh rendering results on the TalkBody4D dataset.

dataset. This dataset includes arm motions, leg motions, and full-body motions of human subjects with diverse skin tones and body types. The Tab. 1 presents a quality com-

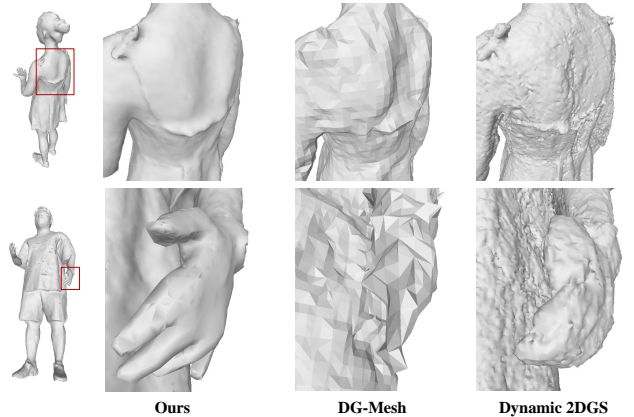


Figure 8. Our method produces smoother and more realistic surface geometry while maintaining topological consistency.

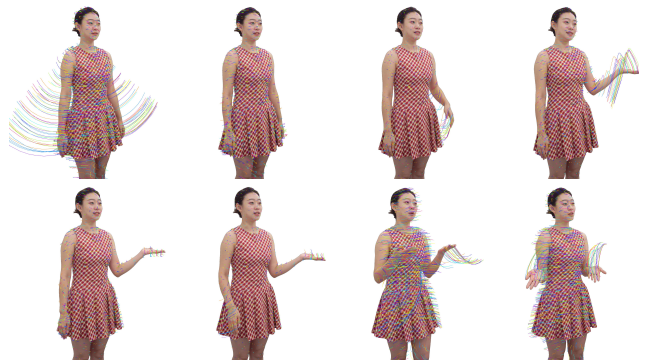


Figure 9. Tracking results on the TalkBody4D dataset. Our method produces stable and accurate keypoint trajectories.

parison of the Gaussian rendering results.

For mesh quality evaluation, we use Chamfer Distance and Earth Mover’s Distance to measure the reconstruction error relative to the ground-truth mesh. As shown in the Fig. 6, our method produces meshes with smoother and more realistic vertex distributions compared to other ap-

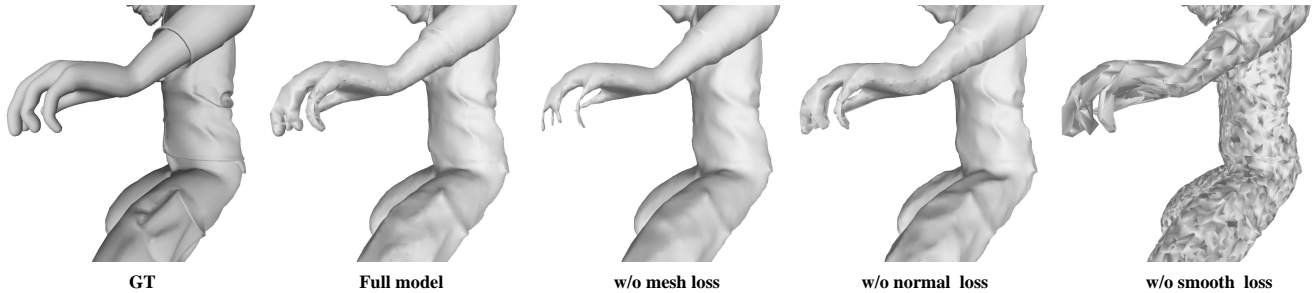


Figure 10. Ablation study on mesh reconstruction. Visual comparison shows that mesh loss, normal loss, and smoothness loss all contribute to more accurate and artifact-free reconstructions.

proaches. Compared with other methods, our approach is distinguished by producing reconstructed mesh sequences that preserve the consistent topology. As shown in Tab. 1, where our method outperforms the baselines.

For tracking accuracy, we processed the original mesh models from the MIX-TAG dataset and recorded motion sequences of representative mesh vertices as ground-truth trajectories. We use Mean Squared Error (MSE) to measure the difference between the algorithm’s tracking results and the ground truth, representing tracking accuracy. The tracking accuracy results are reported in the Tab. 1.

We also evaluated reconstruction results on TalkBody4D[3] dataset. Since this dataset does not provide ground-truth mesh models, we cannot quantitatively compare reconstruction or tracking accuracy. The mesh rendering results are shown in the Fig. 7, with detailed metrics reported in the Tab. 2.

We compared the reconstructed meshes; the reconstruction results and details are presented in the Fig. 8, showing that our method generates more realistic and smoother meshes while maintaining the consistent topology. We visualized tracking results on TalkBody4D, as shown in the Fig. 9. It can be observed that our method produces stable tracking.

Method	PSNR _m ↑	SSIM _m ↑	LPIPS _m ↓
DG-Mesh	24.90	0.91	0.097
Dynamic-2DGS	23.58	0.90	0.081
Ours	26.82	0.93	0.077

Table 2. Mesh rendering quality on the TalkBody4D dataset.

4.3. Ablations

We conducted ablation studies on the MIX-TAG dataset to analyze the contribution of different losses and structural components. We first validated the effectiveness of various static reconstruction losses and the proposed topology-preserving densification and pruning (D&P) module, with quantitative results summarized in Tab. 3. As shown in Fig. 10, removing the smooth loss leads to surface artifacts, while the mesh and normal losses are crucial for accurate geometry recovery. In addition, removing the D&P module results in degraded reconstruction fidelity, verifying its role in maintaining manifold topology and preserving fine sur-

face details. We further evaluated the temporal consistency losses, with results reported in Tab. 4. The results show that the length, rigidity, and rotation constraints jointly ensure smooth deformation across frames. Removing any of these terms causes noticeable degradation in both reconstruction accuracy and tracking stability, confirming their complementary effects.

Method	PSNR _{gs} ↑	PSNR _m ↑	CD ↓	EMD ↓
Full model	32.90	29.75	0.360	0.10703
w/o mesh loss	27.70	27.41	0.396	0.11238
w/o normal loss	27.42	28.21	0.384	0.11038
w/o smooth loss	28.82	26.55	0.408	0.11231
w/o D&P [†]	30.22	28.68	0.378	0.10984

Table 3. Ablation study of static reconstruction losses. Removing mesh, normal, or smoothness loss degrades reconstruction fidelity and mesh quality. [†] D&P denotes the topology-preserving densification and pruning strategy.

Method	Tracking MSE ↓
Full model	0.000368
w/o length loss	0.000412
w/o rigid loss	0.000395
w/o rot loss	0.000372

Table 4. Ablation study of temporal consistency loss functions. Removing rigid, rotation, or isotropic constraints reduces tracking accuracy.

5. Conclusion

We present a topology-aware dynamic reconstruction and tracking framework based on 3D Gaussian Splatting. The method reconstructs topology-consistent meshes and supports precise 3D keypoint tracking across dynamic sequences. Our method bridges the gap between Gaussian-based and mesh-based representations for dynamic reconstruction. The topology-preserving densification and pruning method ensures the manifold topology while increasing the number of Gaussians. Furthermore, a series of regularization terms is introduced to achieve temporally smooth deformation of Gaussian parameters while preserving topology. Experimental results demonstrate that our method outperforms existing approaches on both synthetic

and real datasets, achieving significant improvements in mesh reconstruction accuracy and keypoint tracking precision. This provides a high-fidelity and cost-effective solution for downstream tasks such as animation production.

Limitation: Our method demonstrates strong performance in dynamic mesh modeling and tracking, effectively handling non-rigid deformations while maintaining consistent topology. However, it should be noted that the current framework is primarily designed for scenarios with stable topological relationships. It lacks sufficient adaptability to handle cases with drastic topological changes, such as clothing tears or object splits. This limitation restricts its applicability in more complex dynamic scenes. Future research could explore extending the method to accommodate dynamic objects with changing topology. We believe progress in this direction will broaden the method’s applicability and increase its practical value.

References

- [1] Jad Abou-Chakra, Krishan Rana, Feras Dayoub, and Niko Sünderhauf. Physically embodied gaussian splatting: A real-time correctable world model for robotics. *arXiv preprint arXiv:2406.10788*, 2024. 3
- [2] Hanlin Chen, Chen Li, and Gim Hee Lee. Neusg: Neural implicit surface reconstruction with 3d gaussian splatting guidance. *arXiv preprint arXiv:2312.00846*, 2023. 1
- [3] Jianchuan Chen, Jingchuan Hu, Gaige Wang, Zhonghua Jiang, Tiansong Zhou, Zhiwen Chen, and Chengfei Lv. Taoavatar: Real-time lifelike full-body talking avatars for augmented reality via 3d gaussian splatting. In *Proceedings of the Computer Vision and Pattern Recognition Conference*, pages 10723–10734, 2025. 6, 8
- [4] Yihang Chen, Qianyi Wu, Weiyao Lin, Mehrtash Harandi, and Jianfei Cai. Hac: Hash-grid assisted context for 3d gaussian splatting compression. In *European Conference on Computer Vision*, pages 422–438. Springer, 2024. 3
- [5] Yihang Chen, Mengyao Li, Qianyi Wu, Weiyao Lin, Mehrtash Harandi, and Jianfei Cai. Pcgsg: Progressive compression of 3d gaussian splatting. *arXiv preprint arXiv:2503.08511*, 2025. 3
- [6] Yixiao Chen, Bin Liang, Hanzhi Guo, Yongqing Cheng, Jiayi Zhao, and Dongdong Weng. Ps-gsg: Gaussian splatting for multi-view photometric stereo. *arXiv preprint arXiv:2507.18231*, 2025. 2
- [7] Yihang Chen, Qianyi Wu, Weiyao Lin, Mehrtash Harandi, and Jianfei Cai. Hac++: Towards 100x compression of 3d gaussian splatting. *arXiv preprint arXiv:2501.12255*, 2025. 3
- [8] Euntae Choi and Sungjoo Yoo. Phys3dgs: Physically-based 3d gaussian splatting for inverse rendering. *arXiv preprint arXiv:2409.10335*, 2024. 3
- [9] Alvaro Collet, Ming Chuang, Pat Sweeney, Don Gillett, Dennis Evseev, David Calabrese, Hugues Hoppe, Adam Kirk, and Steve Sullivan. High-quality streamable free-viewpoint video. *ACM Transactions on Graphics (ToG)*, 34(4):1–13, 2015. 1
- [10] Xiaonuo Dongye, Hanzhi Guo, Le Luo, Haiyan Jiang, Yihua Bao, Zeyu Tian, and Dongdong Weng. Lodavatar: Hierarchical embedding and adaptive levels of detail with gaussian splatting for enhanced human avatars. *arXiv preprint arXiv:2410.20789*, 2024. 2
- [11] Sara Fridovich-Keil, Alex Yu, Matthew Tancik, Qinhong Chen, Benjamin Recht, and Angjoo Kanazawa. Plenoxels: Radiance fields without neural networks. In *Proceedings of the IEEE/CVF conference on computer vision and pattern recognition*, pages 5501–5510, 2022. 2
- [12] Antoine Guédon and Vincent Lepetit. Sugar: Surface-aligned gaussian splatting for efficient 3d mesh reconstruction and high-quality mesh rendering. In *Proceedings of the IEEE/CVF Conference on Computer Vision and Pattern Recognition*, pages 5354–5363, 2024. 1
- [13] Rana Hanocka, Gal Metzer, Raja Giryes, and Daniel Cohen-Or. Point2mesh. *ACM Transactions on Graphics*, 39(4), 2020. 1
- [14] Hugues Hoppe. New quadric metric for simplifying meshes with appearance attributes. In *Proceedings Visualization’99 (Cat. No. 99CB37067)*, pages 59–510. IEEE, 1999. 5
- [15] Liangxiao Hu, Hongwen Zhang, Yuxiang Zhang, Boyao Zhou, Boning Liu, Shengping Zhang, and Liqiang Nie. Gaussianavatar: Towards realistic human avatar modeling from a single video via animatable 3d gaussians. In *Proceedings of the IEEE/CVF conference on computer vision and pattern recognition*, pages 634–644, 2024. 3
- [16] Binbin Huang, Zehao Yu, Anpei Chen, Andreas Geiger, and Shenghua Gao. 2d gaussian splatting for geometrically accurate radiance fields. In *ACM SIGGRAPH 2024 conference papers*, pages 1–11, 2024. 2
- [17] Yuheng Jiang, Zhehao Shen, Penghao Wang, Zhuo Su, Yu Hong, Yingliang Zhang, Jingyi Yu, and Lan Xu. Hifi4g: High-fidelity human performance rendering via compact gaussian splatting. In *Proceedings of the IEEE/CVF conference on computer vision and pattern recognition*, pages 19734–19745, 2024. 2
- [18] Yuheng Jiang, Chengcheng Guo, Yize Wu, Yu Hong, Shengkun Zhu, Zhehao Shen, Yingliang Zhang, Shaohui Jiao, Zhuo Su, Lan Xu, et al. Topology-aware optimization of gaussian primitives for human-centric volumetric videos. *arXiv preprint arXiv:2509.07653*, 2025.
- [19] HyunJun Jung, Nikolas Brasch, Jifei Song, Eduardo Pérez-Pellitero, Yiren Zhou, Zhihao Li, Nassir Navab, and Benjamin Busam. Deformable 3d gaussian splatting for animatable human avatars. *CoRR*, 2023. 2
- [20] Bernhard Kerbl, Georgios Kopanas, Thomas Leimkühler, and George Drettakis. 3d gaussian splatting for real-time radiance field rendering. *ACM Trans. Graph.*, 42(4):139–1, 2023. 1, 2, 4
- [21] Alexander Kirillov, Eric Mintun, Nikhila Ravi, Hanzi Mao, Chloe Rolland, Laura Gustafson, Tete Xiao, Spencer Whitehead, Alexander C Berg, Wan-Yen Lo, et al. Segment anything. In *Proceedings of the IEEE/CVF international conference on computer vision*, pages 4015–4026, 2023. 4
- [22] Samuli Laine, Janne Hellsten, Tero Karras, Yeongho Seol, Jaakko Lehtinen, and Timo Aila. Modular primitives for

- high-performance differentiable rendering. *ACM Transactions on Graphics (ToG)*, 39(6):1–14, 2020. 4
- [23] Xuanchen Li, Yuhao Cheng, Xingyu Ren, Haozhe Jia, Di Xu, Wenhan Zhu, and Yichao Yan. Topo4d: Topology-preserving gaussian splatting for high-fidelity 4d head capture. In *European Conference on Computer Vision*, pages 128–145. Springer, 2024. 3, 4
- [24] Zhe Li, Zerong Zheng, Lizhen Wang, and Yebin Liu. Animatable gaussians: Learning pose-dependent gaussian maps for high-fidelity human avatar modeling. In *Proceedings of the IEEE/CVF conference on computer vision and pattern recognition*, pages 19711–19722, 2024. 3
- [25] Isabella Liu, Hao Su, and Xiaolong Wang. Dynamic gaussians mesh: Consistent mesh reconstruction from dynamic scenes. In *The Thirteenth International Conference on Learning Representations*, 2024. 2, 3, 4
- [26] Xiangrui Liu, Xinju Wu, Pingping Zhang, Shiqi Wang, Zhu Li, and Sam Kwong. Compgs: Efficient 3d scene representation via compressed gaussian splatting. In *Proceedings of the 32nd ACM International Conference on Multimedia*, pages 2936–2944, 2024. 3
- [27] Xiangrui Liu, Xinju Wu, Shiqi Wang, Zhu Li, and Sam Kwong. Compgs++: Compressed gaussian splatting for static and dynamic scene representation. *arXiv preprint arXiv:2504.13022*, 2025. 3
- [28] WE Lorens. A high resolution 3d surface construction algorithm. *Proc. Siggraph* 87, 1987. 3
- [29] Jonathon Luiten, Georgios Kopanas, Bastian Leibe, and Deva Ramanan. Dynamic 3d gaussians: Tracking by persistent dynamic view synthesis. In *2024 International Conference on 3D Vision (3DV)*, pages 800–809. IEEE, 2024. 2, 6
- [30] Lars Mescheder, Michael Oechsle, Michael Niemeyer, Sebastian Nowozin, and Andreas Geiger. Occupancy networks: Learning 3d reconstruction in function space. In *Proceedings of the IEEE/CVF conference on computer vision and pattern recognition*, pages 4460–4470, 2019. 2
- [31] Ben Mildenhall, Pratul P Srinivasan, Matthew Tancik, Jonathan T Barron, Ravi Ramamoorthi, and Ren Ng. Nerf: Representing scenes as neural radiance fields for view synthesis. *Communications of the ACM*, 65(1):99–106, 2021. 2
- [32] Arthur Moreau, Jifei Song, Helisa Dharmo, Richard Shaw, Yiren Zhou, and Eduardo Pérez-Pellitero. Human gaussian splatting: Real-time rendering of animatable avatars. In *Proceedings of the IEEE/CVF conference on computer vision and pattern recognition*, pages 788–798, 2024. 3
- [33] Thomas Müller, Alex Evans, Christoph Schied, and Alexander Keller. Instant neural graphics primitives with a multiresolution hash encoding. *ACM transactions on graphics (TOG)*, 41(4):1–15, 2022. 2
- [34] Jeong Joon Park, Peter Florence, Julian Straub, Richard Newcombe, and Steven Lovegrove. Deepsdf: Learning continuous signed distance functions for shape representation. In *Proceedings of the IEEE/CVF conference on computer vision and pattern recognition*, pages 165–174, 2019. 2
- [35] Keunhong Park, Utkarsh Sinha, Jonathan T Barron, Sofien Bouaziz, Dan B Goldman, Steven M Seitz, and Ricardo Martin-Brualla. Nerfies: Deformable neural radiance fields. In *Proceedings of the IEEE/CVF international conference on computer vision*, pages 5865–5874, 2021. 3
- [36] Keunhong Park, Utkarsh Sinha, Peter Hedman, Jonathan T Barron, Sofien Bouaziz, Dan B Goldman, Ricardo Martin-Brualla, and Steven M Seitz. Hypernerf: a higher-dimensional representation for topologically varying neural radiance fields. *ACM Transactions on Graphics (TOG)*, 40(6):1–12, 2021.
- [37] Albert Pumarola, Enric Corona, Gerard Pons-Moll, and Francesc Moreno-Noguer. D-nerf: Neural radiance fields for dynamic scenes. In *Proceedings of the IEEE/CVF conference on computer vision and pattern recognition*, pages 10318–10327, 2021. 3
- [38] Shenhan Qian, Tobias Kirschstein, Liam Schoneveld, Davide Davoli, Simon Giebenhain, and Matthias Nießner. Gaussianavatars: Photorealistic head avatars with rigged 3d gaussians. In *Proceedings of the IEEE/CVF Conference on Computer Vision and Pattern Recognition*, pages 20299–20309, 2024. 3
- [39] Shunsuke Saito, Gabriel Schwartz, Tomas Simon, Junxuan Li, and Giljoo Nam. Relightable gaussian codec avatars. In *Proceedings of the IEEE/CVF Conference on Computer Vision and Pattern Recognition*, pages 130–141, 2024. 2
- [40] Jiayang Tang, Hang Zhou, Xiaokang Chen, Tianshu Hu, Errui Ding, Jingdong Wang, and Gang Zeng. Delicate textured mesh recovery from nerf via adaptive surface refinement. In *Proceedings of the IEEE/CVF International Conference on Computer Vision*, pages 17739–17749, 2023. 3
- [41] Graham M Treece, Richard W Prager, and Andrew H Gee. Regularised marching tetrahedra: improved iso-surface extraction. *Computers & Graphics*, 23(4):583–598, 1999. 3
- [42] Peng Wang, Lingjie Liu, Yuan Liu, Christian Theobalt, Taku Komura, and Wenping Wang. Neus: Learning neural implicit surfaces by volume rendering for multi-view reconstruction. *arXiv preprint arXiv:2106.10689*, 2021. 1, 2
- [43] Yiming Wang, Qin Han, Marc Habermann, Kostas Daniilidis, Christian Theobalt, and Lingjie Liu. Neus2: Fast learning of neural implicit surfaces for multi-view reconstruction. In *Proceedings of the IEEE/CVF International Conference on Computer Vision*, pages 3295–3306, 2023. 6
- [44] Tianyi Xie, Zeshun Zong, Yuxing Qiu, Xuan Li, Yutao Feng, Yin Yang, and Chenfanfu Jiang. Physgaussian: Physics-integrated 3d gaussians for generative dynamics. In *Proceedings of the IEEE/CVF Conference on Computer Vision and Pattern Recognition*, pages 4389–4398, 2024. 3
- [45] Yuelang Xu, Benwang Chen, Zhe Li, Hongwen Zhang, Lizhen Wang, Zerong Zheng, and Yebin Liu. Gaussian head avatar: Ultra high-fidelity head avatar via dynamic gaussians. In *Proceedings of the IEEE/CVF Conference on Computer Vision and Pattern Recognition*, 2024. 3
- [46] Yuxuan Xue, Bharat Lal Bhatnagar, Riccardo Marin, Nikolaos Sarafianos, Yuanlu Xu, Gerard Pons-Moll, and Tony Tung. Nsf: Neural surface fields for human modeling from monocular depth. In *Proceedings of the IEEE/CVF international conference on computer vision*, pages 15049–15060, 2023. 1

- [47] Lior Yariv, Jiatao Gu, Yoni Kasten, and Yaron Lipman. Volume rendering of neural implicit surfaces. *Advances in neural information processing systems*, 34:4805–4815, 2021. [2](#)
- [48] Mingqiao Ye, Martin Danelljan, Fisher Yu, and Lei Ke. Gaussian grouping: Segment and edit anything in 3d scenes. In *ECCV*, 2024. [2](#)
- [49] Shuai Zhang, Guanjun Wu, Zhoufeng Xie, Xinggang Wang, Bin Feng, and Wenyu Liu. Dynamic 2d gaussians: Geometrically accurate radiance fields for dynamic objects. *arXiv preprint arXiv:2409.14072*, 2024. [2](#), [3](#)
- [50] Chengwei Zheng, Lixin Xue, Juan Zarate, and Jie Song. Gaustar: Gaussian surface tracking and reconstruction. In *Proceedings of the Computer Vision and Pattern Recognition Conference*, pages 16543–16553, 2025. [2](#), [3](#)

TagSplat: Topology-Aware Gaussian Splatting for Dynamic Mesh Modeling and Tracking

Supplementary Material

A. Initialization of Gaussian Primitives

The initialization of Gaussian primitives is a crucial step that determines the effectiveness of subsequent optimization. Since Gaussian rendering optimization is inherently non-convex, the quality of the initial Gaussian model largely affects the reconstruction fidelity and convergence speed. In recent years, multi-view mesh reconstruction has developed several mature methods. To obtain a high-quality initial topology, we first perform multi-view geometric reconstruction on the first frame. This produces a dense 3D mesh model. The Gaussian model is then initialized based on the reconstructed mesh.

Let the reconstructed mesh be denoted as $\mathcal{M} = (\mathcal{V}, \mathcal{F})$, where $\mathcal{V} = \{\mathbf{v}_i \in \mathbb{R}^3\}$ is the set of vertices and $\mathcal{F} = \{\mathbf{f}_i \in \mathbb{Z}^3\}$ is the set of faces. We initialize the position parameter $\mathbf{p}_i \in \mathbb{R}^3$ of each Gaussian primitive by the corresponding vertex position \mathbf{v}_i , that is, $\mathbf{p}_i = \mathbf{v}_i$.

The color parameter $\mathbf{c}_i \in \mathbb{R}^3$ is directly initialized using the RGB color of the corresponding mesh vertex. The opacity parameter α_i is uniformly initialized to a constant value of 1. The rotation parameter $\mathbf{R}_i \in SO(3)$ is initialized based on the vertex normal \mathbf{n}_i . Specifically, \mathbf{n}_i is used as the local coordinate system’s z -axis direction.

For the scale parameter $\mathbf{s}_i = (s_{i,x}, s_{i,y}, s_{i,z})^\top$, we initialize the $s_{i,x}$ and $s_{i,y}$ based on the distance to neighboring vertices to ensure coverage. Meanwhile, the the scale factor $s_{i,z}$ along the surface normal direction is set to a small value ϵ , so that the Gaussian primitive closely adheres to the surface:

$$s_{i,z} = \epsilon \ll s_{i,x}, s_{i,y} \quad (1)$$

Finally, the initial set of Gaussians can be represented as $\mathcal{G} = \left(\{(\mathbf{p}_i, \mathbf{R}_i, \mathbf{s}_i, \mathbf{c}_i, \alpha_i)\}_{i=1}^{|\mathcal{V}|}, \mathcal{F} \right)$. Here, \mathcal{F} represents the face index information inherited from the mesh model, which defines the topological connections between vertices. This topology can be employed in designing consistency regularization, facilitating the preservation of local geometric coherence of the target surface during Gaussian optimization.

B. Detail of topology-preserving densification and pruning process

We propose a method that preserves the manifold topology of the model during the densification and pruning processes. The goal is to balance geometric detail and structural quality. Specifically, the topology-preserving densifi-

Algorithm 1: Topology-preserving Gaussian Densification

Input: Gaussian scales S , other Gaussian parameters P , topology \mathcal{T} , vertex gradients G , gradients thresholds τ_g , scale thresholds τ_s

Output: Updated \mathcal{T}, S, P

foreach $face\ f = (v_1, v_2, v_3) \in \mathcal{T}$ **do**

$g_f \leftarrow \frac{1}{3}(G_{v_1} + G_{v_2} + G_{v_3})$

if $g_f > \tau_g$ **then**

$\bar{s} \leftarrow \frac{1}{3}(S_{v_1} + S_{v_2} + S_{v_3})$

if $\bar{s} < \tau_s$ **then**

$s_{new} \leftarrow \bar{s}$

else

$s_{new} \leftarrow \frac{1}{2}\bar{s}$

$S_{v_i} \leftarrow \frac{1}{2}S_{v_i}, i = 1, 2, 3$

$p_{new} \leftarrow \frac{1}{3}(P_{v_1} + P_{v_2} + P_{v_3})$

$\mathcal{T} \leftarrow \mathcal{T} \cup \text{new_connections}$

$S \leftarrow S \cup s_{new}, P \leftarrow P \cup p_{new}$

Algorithm 2: Topology-preserving Gaussian Pruning (simplified)

Input: Gaussian parameters \mathcal{G} , topology \mathcal{T} , opacity threshold ϵ

Output: Updated \mathcal{G} and \mathcal{T}

foreach $g_i \in \mathcal{G}$ **do**

if $\alpha_i < \epsilon$ **or** $IsTooLarge(g_i)$ **then**

$\mathcal{N}_i \leftarrow$ 1-ring neighbors of g_i in \mathcal{T}

$p \leftarrow \arg \min_{g_j \in \mathcal{N}_i} \text{CollapseCost}(g_i, g_j)$

$\mathcal{T} \leftarrow \text{EdgeCollapse}(\mathcal{T}, p)$

$\mathcal{G} \leftarrow \text{Remove}(\mathcal{G}, g_i)$

cation strategy (see Algorithm 1) enhances geometric details in sparse regions to improve reconstruction realism, while the topology-preserving pruning strategy (see Algorithm 2) removes redundant Gaussian primitives and maintains the integrity of the final topology. Working together, these two processes ensure the generation of high-quality mesh models with consistent topology.

C. Loss function weights

We designed two sets of loss functions for the first frame and the subsequent frames. Each set combines multiple sub-

losses with weighted sums to balance different optimization objectives. The specific weight configurations used during training are summarized in the Tab. 1.

Loss	Weight
\mathcal{L}_c^{gs}	1.0
\mathcal{L}_c^{mesh}	1.0
\mathcal{L}_m^{gs}	3.0
\mathcal{L}_m^{mesh}	3.0
\mathcal{L}_{2d}	1.0
\mathcal{L}_{lap}	5.0
\mathcal{L}_n	1.0
\mathcal{L}_{len}	4.0
\mathcal{L}_{rigid}	4.0
\mathcal{L}_{rot}	20.0

Table 1. Loss Function Weights.

D. Introduction to the MIX-TAG Dataset

The MIX-TAG dataset comprises three dynamic human subjects: Worker, Dancer, and Boxer. To construct the dataset, we developed an automated data acquisition pipeline in Blender, deploying 42 uniformly distributed virtual cameras in each scene to perform frame-by-frame multi-view rendering of the animation sequences. In addition to RGB images, we simultaneously generated accurate binary masks for each frame. All rendered images have a resolution of 1080×1080.

In terms of sequence composition, Worker contains a 90-frame animation, while Dancer and Boxer each consist of 130 frames. These sequences include a wide range of challenging motion patterns, such as full-body coordinated motion, large leg swings, and torso rotations, ensuring the diversity and comprehensiveness of the dataset.

E. More results on the MIX-TAG dataset

Fig. 1, Fig. 2 and Fig. 3 present both the Gaussian rendering results and the mesh reconstruction results obtained from models trained on the MIX-TAG dataset. Our method is compared with several Gaussian-based reconstruction approaches, including Dynamic 3DGS, DG-Mesh, Deformable-GS, and Dynamic 2DGS. The experimental results clearly demonstrate that, compared with existing baselines, our method achieves superior performance in both mesh reconstruction accuracy and rendering quality.

F. More results on the Talkbody4D dataset

Fig. 4 presents additional results on the real dataset. We compare our method with DG-Mesh and Dynamic 2DGS in

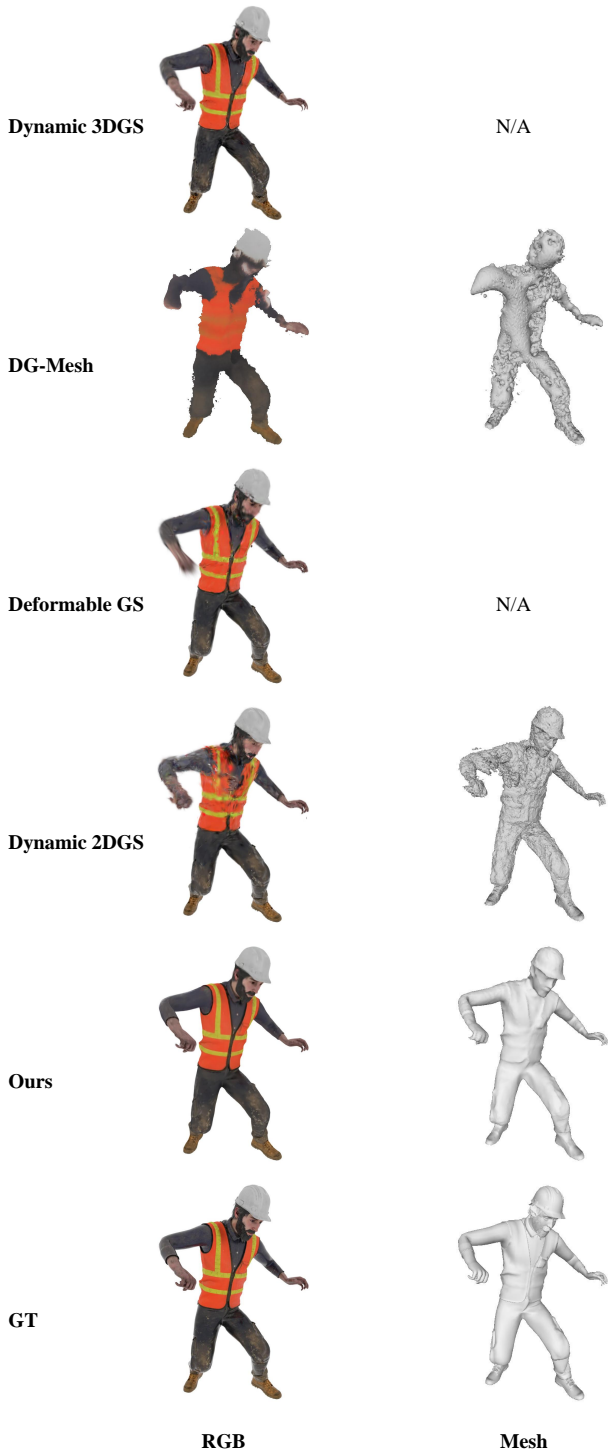


Figure 1. Comparison of training results for the Worker object.

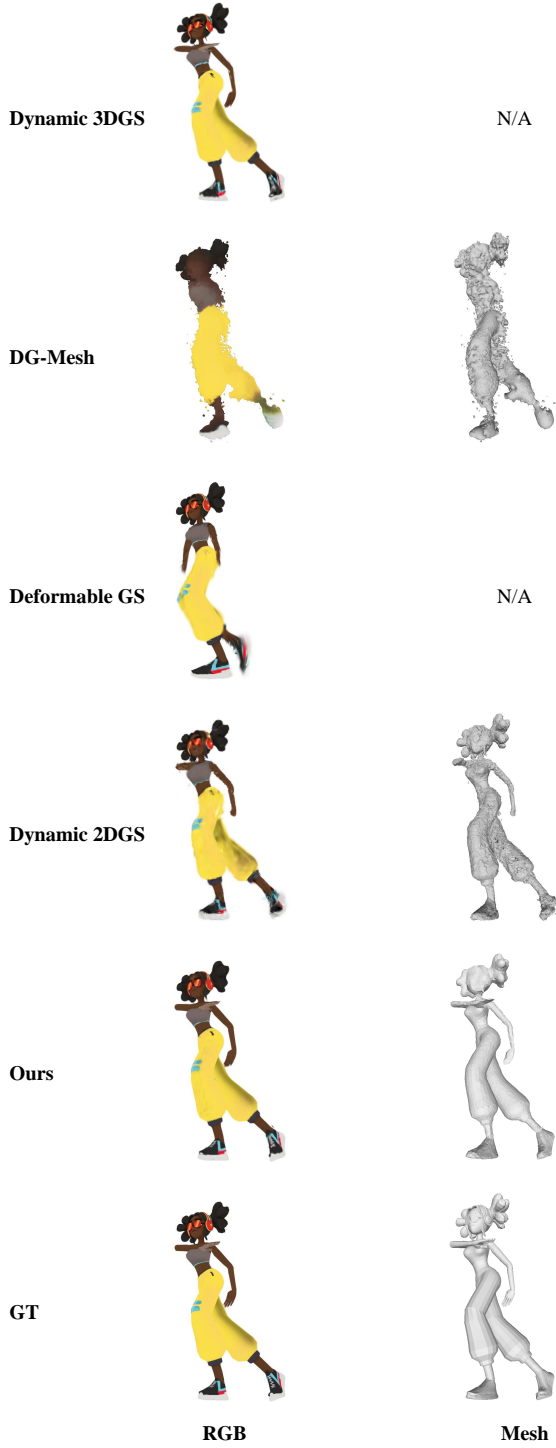


Figure 2. Comparison of training results for the Dancer object.

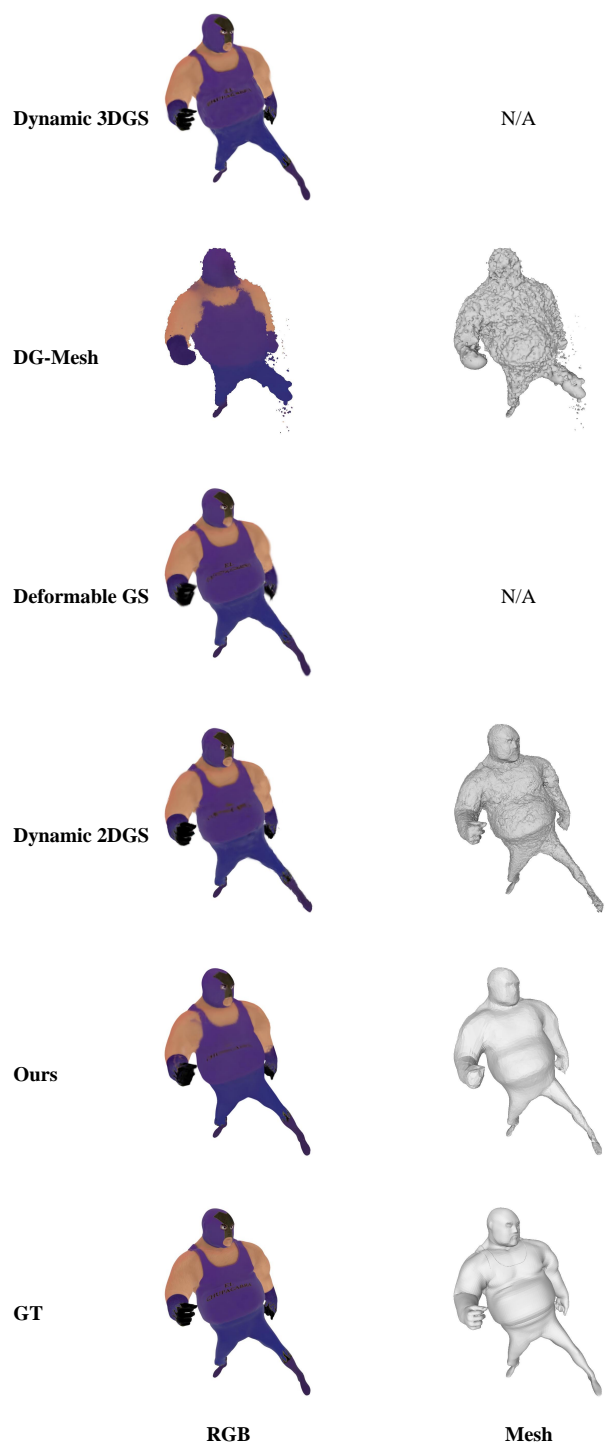


Figure 3. Comparison of training results for the Boxer object.

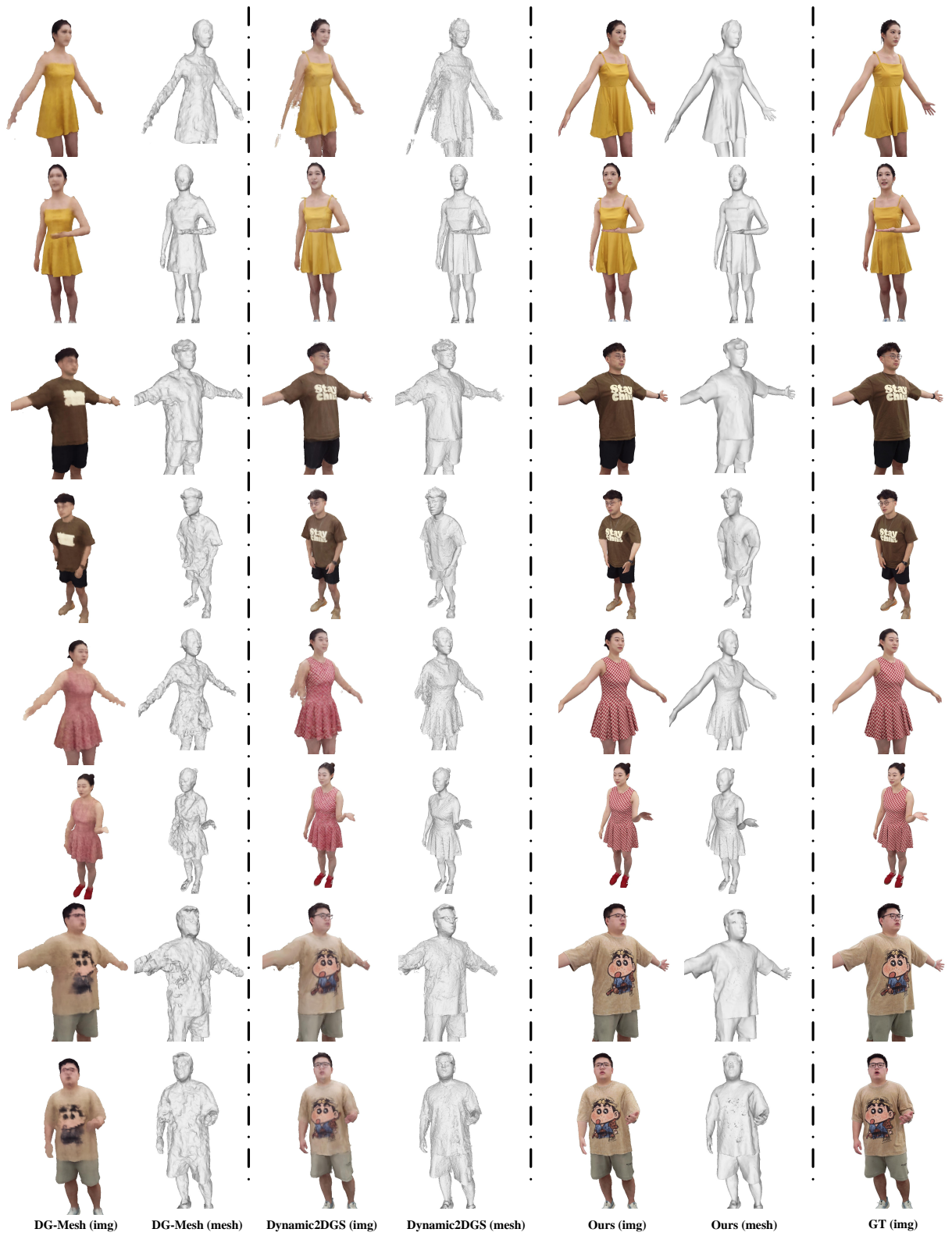


Figure 4. Comparison of training results on Talkbody4D dataset.

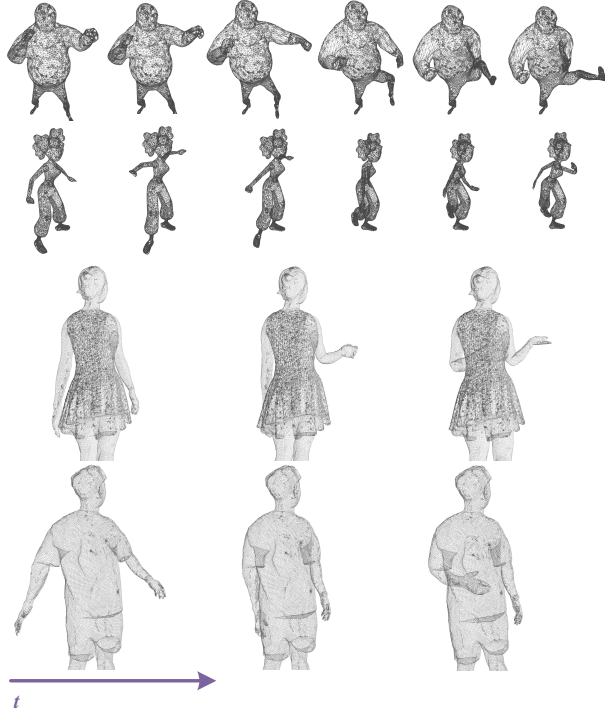


Figure 5. The topology of the mesh sequence.

terms of mesh rendering and mesh reconstruction. The results show that our approach produces meshes with higher geometric fidelity, better structural coherence, and smoother surfaces. Furthermore, the meshes render results exhibit more realistic appearance compared with existing methods.



Figure 6. Model Editing Result.

G. Topology-consistent model sequence

A key advantage of our method is its ability to reconstruct a sequence of topology-consistent 3D models from multi-view videos of dynamic objects. This property is essen-

tial for downstream tasks such as geometric analysis, motion processing, and physical simulation. As shown in Fig. 5, the reconstructed sequence maintains identical vertex counts and connectivity across all frames, ensuring consistent mesh topology throughout the motion.

H. Efficient Editing of Dynamic Sequences via Consistent Topology

Our method ultimately produces topology-consistent Gaussian and mesh sequences of the target object. The globally consistent topology allows reliable 3D keypoint tracking and significantly simplifies the editing of dynamic sequences. Specifically, since all frames share the same topology, editing a single frame and propagating the changes across the sequence is sufficient to achieve global adjustments to the dynamic model. The results of model editing are shown in Fig. 6.